NASA SP-8013

NASA
SPACE VEHICLE
DESIGN CRITERIA
(ENVIRONMENT)

METEOROID ENVIRONMENT MODEL - 1969 [NEAR EARTH TO LUNAR SURFACE]

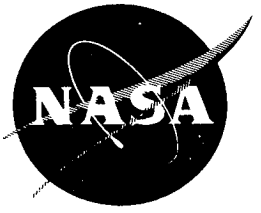

March 1969

NATIONAL AERONAUTICS AND SPACE ADMINISTRATION

FOREWORD

NASA experience has indicated a need for uniform design criteria for space vehicles. Accordingly, criteria are being developed in the following areas of technology:

Environment
Structures
Guidance and Control
Chemical Propulsion

Individual components will be issued as separate monographs as soon as they are completed. A list of all previously issued monographs in this series can be found on the last page of this publication.

These monographs are to be regarded as guides to design and not as NASA requirements, except as may be specified in formal project specifications. It is expected, however, that the criteria sections of these documents, revised as experience may indicate to be desirable, eventually will become uniform design requirements for NASA space vehicles.

This monograph was prepared by B. G. Cour-Palais of the NASA Manned Spacecraft Center with the assistance of an ad hoc committee, consisting of Fred L. Whipple, Chairman; B. G. Cour-Palais; C. T. D'Aiutolo; C. C. Dalton; J. S. Dohnanyi; M. Dubin; V. C. Frost; W. H. Kinard; I. J. Loeffler; R. J. Naumann; C. R. Nysmith; and R. C. Savin.

Comments concerning the technical content of these monographs will be welcomed by the National Aeronautics and Space Administration, Office of Advanced Research and Technology (Code RVA), Washington, D.C. 20546.

March 1969

For sale by the Clearinghouse for Federal Scientific and Technical Information
Springfield, Virginia 22151 – Price $3.00

CONTENTS

METEOROID ENVIRONMENT MODEL - 1969 (NEAR EARTH TO LUNAR SURFACE)

1. INTRODUCTION

Meteoroids are solid particles moving in interplanetary space and originate from both cometary and asteroidal sources. Because of their velocity, density, and mass, meteoroids can cause damage to vehicles operating in space. The type and extent of the damage depend upon vehicle size, vehicle structural configuration, and exposure time in space, as well as on meteoroid characteristics. Meteoroid impact on a space vehicle can result in damage such as the puncture of a pressurized cabin, radiator, or propellant tank; the deterioration of windows, optical surfaces, and thermal balance coatings by cratering and spallation; or reduction of heat shield effectiveness. Other possible impact effects include damage to antenna systems, thruster nozzles, and electrical leads.

This monograph treats only the meteoroid environment of cometary origin in the mass range between 10^{-12} and 1 gram at one astronomical unit (1 A.U.) from the Sun near the ecliptic plane. Also included are the lunar ejecta created by the impact of cometary particles on the lunar surface. In this region (1 A.U.) the contribution of asteroidal particles to the total meteoroid population is considered to be negligible. The meteoroid and the lunar surface ejecta flux-mass models and the associated density and velocity characteristics presented herein are for engineering application in the design of space vehicles for near-Earth orbit, cislunar, lunar orbit, and lunar surface missions.

The meteoroid environment in interplanetary space and the design of vehicle systems for protection against meteoroids will be the subjects of separate monographs.

For purposes of identification in this monograph, "meteoroids" are classified as sporadics when their orbits are random and as streams (or showers) when a number of meteoroids have nearly identical orbits. A "meteor" is the light phenomena associated with the interaction of a meteoroid with the Earth's atmosphere. The portion that survives interaction with the atmosphere and is found on the surface of the Earth is a "meteorite."

2. STATE OF THE ART

Present knowledge of both the occurrence and physical properties of meteoroids considered important for near-Earth, cislunar, and lunar missions is based on observations of meteors made by Earth-based photographic and radar (also called radio) techniques and on direct measurements of the near-Earth meteoroid flux (number of particles per unit area per unit

time) by instrumented sounding rockets and spacecraft. References 1 through 7 review observations of meteors and direct measurements of meteoroid impacts on and penetrations of instrumented spacecraft.

2.1 Observations and Measurements

2.1.1 Photographic Observations

Photographic observations have furnished the best information on meteors to date. The meteoroid population is inferred from analysis of such observations. References 8 through 10 contain the data generally conceded as providing the best estimates of the flux of meteors as a function of their luminosity. Large temporal and spatial variations are apparent from the observations and these variations form the basis for the description of the stream meteoroid environment. The meteoroid population inferred from these observations, however, is subject to error because of several limitations in the observed data such as the uncertainty in converting the luminosity measurement to mass, the mass range observable, and meteoroid composition and structure.

2.1.2 Radar Observations

A large number of observations of meteors has been obtained from the reflection of radar beams by the ionized meteor trails. References 11,12, and 13 contain some recent reviews of meteor influx rates based on radar observations. Clouds and daylight do not limit sampling periods for these observations as for photography; thus, the radar data should have more statistical significance. However, this technique has the same type of limitations as the photographic and, in addition, a selection effect due to the bias in favor of high velocity meteors and the disturbing effect of wind shear on the ionized trails of the fainter objects. Because of these severe selection effects, the radar technique is considered less reliable than the photographic meteor measurements. The two Earth-based techniques provide information in the meteoroid mass range greater than 10^{-6} gram.

2.1.3 Direct Measurements

Meteoroid detectors mounted on spacecraft and rockets have furnished information on the meteoroid flux in the mass range 10^{-13} to 10^{-6} gram (refs. 4-7). Fluxes in the mass range less than 10^{-7} gram have been detected by acoustic impact (microphone) sensors while fluxes in the mass range of 10^{-9} to 10^{-6} gram have been determined by the detection of complete penetrations (perforations) of thin metallic sheet sensors. Measurements by acoustic impact sensors (ref. 4) indicate a much higher flux of particles having masses less than 10^{-7} gram than do the penetration sensors (refs. 5-7). Although neither the acoustic nor the penetration sensors directly measure the meteoroid mass and velocity, the penetration data are more significant from the design viewpoint since they stem from actual physical damage by meteoroids.

Moreover, the penetration data, although they are subject to error in the conversion from sensor thickness to meteoroid mass, are considered more reliable than either photographic or radar based data.

2.2 Meteoroid Velocity

The geocentric velocity* of meteoroids is expected to range from 11 to 72 km/sec on the basis of celestial mechanics. Analyses of photographic and radar observations of meteors entering the Earth's atmosphere have confirmed this range of meteoroid velocity.

Typical distributions of meteor velocities from photographic measurements (refs. 2,14, and 15) display two velocity peaks. The second peak near 60 km/sec in the distribution is attributed to meteoroids in retrograde orbits, since their higher entry velocities are more easily detectable than the slower direct orbit meteors. This selection effect tends to give a distorted picture of the proportionate number of meteors in direct and retrograde orbits. A velocity distribution based on constant mass as obtained in reference 16 tends to compensate for the velocity bias inherent in the photographic technique. Average velocity values, determined from photographic measurements are: 20 km/sec by Dohnanyi (ref. 16); 19 km/sec by Dalton (ref. 17); 22 km/sec by Whipple (ref. 18); and 30 km/sec by Burbank et al (ref. 19).

The measured radar meteor velocity distributions do not, to the same extent, exhibit the bi-modal shape characteristics of the photographic meteors. Recent unpublished distributions obtained by the Harvard College Observatory and the Smithsonian Astrophysical Observatory, using the radar technique, indicate a higher average velocity for meteoroids smaller than those detectable by the photographic technique. However, a velocity distribution based on constant mass, as for the photographic data (ref. 16), shows that the average velocity derived from the radar distributions decreases to a value nearer that obtained from the photographic measurements.

Accordingly, on the basis of the velocity information primarily from photographic meteor measurements and the assumption of independence of mass and velocity, an average atmospheric entry velocity of 20 km/sec was adopted as the average velocity of sporadic meteoroids. The probability-velocity distribution for this average velocity is given in figure 1.

The average geocentric velocities of stream meteoroids are included in section 2.5.

*Although incorrect, the term "velocity" has been used in the literature to express the speed of meteoroids.

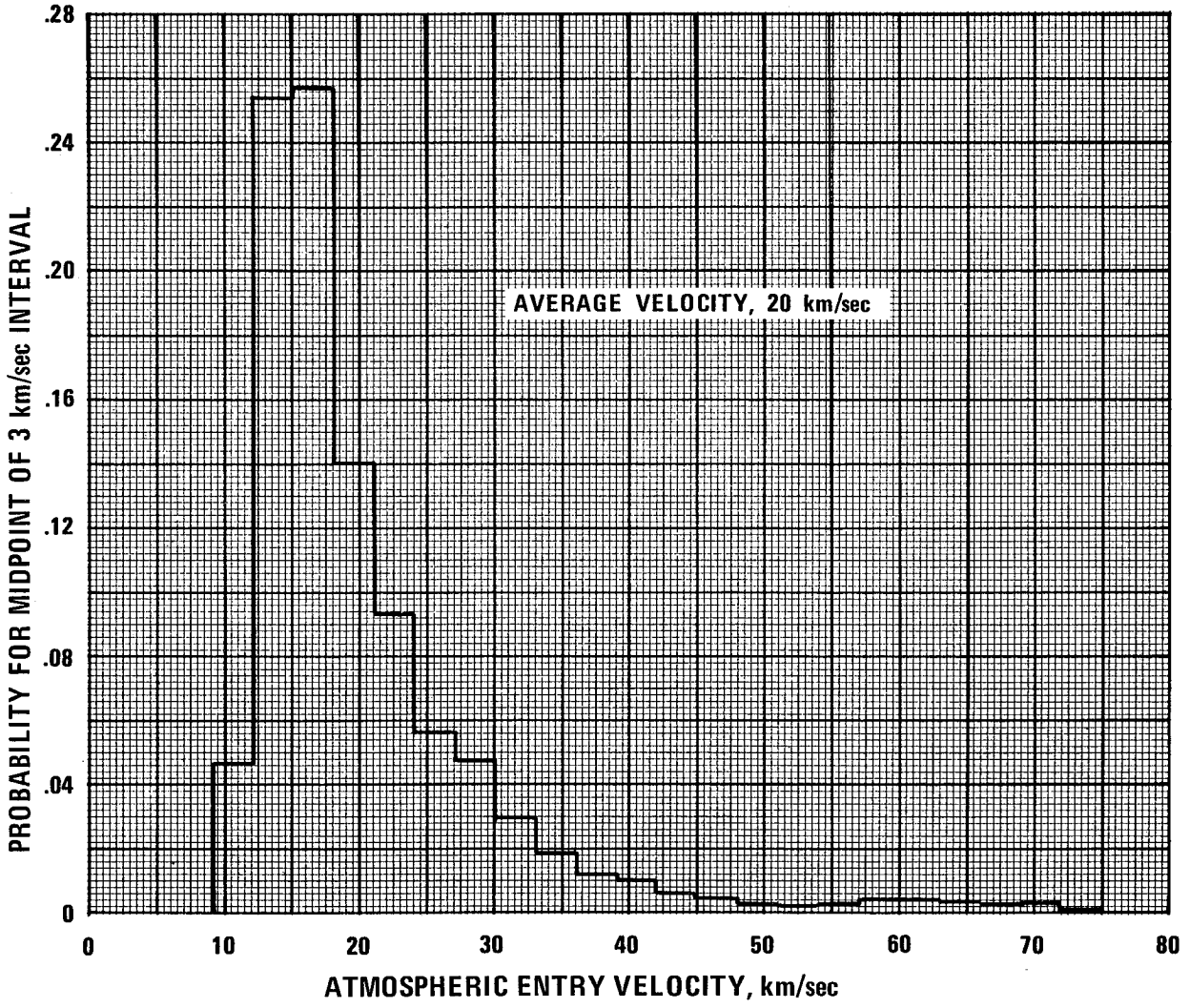

Figure 1.–Probability-velocity distribution for sporadic meteoroids.

2.3 Meteoroid Density

The density of meteoroids is open to serious uncertainty. It, as in the case of meteoroid mass, is not a measured quantity. Although meteorites have been examined – 90% of them generally stoney in character with an average density of 3.5 gms/cm^3 and the remaining 10% iron-nickel with an average density of 7.8 gms/cm^3 – they are generally considered to have been meteoroids of asteroidal origin. The meteoroid density of interest in this monograph is that of particles which result from the break-up of cometary nuclei.

The cometary meteoroid has been described by Whipple (ref.20) as a conglomerate of dust particles bound together by frozen gases or "ices" while Opik, as given in ref. 20, postulated a dust ball. The flux-mass relationship, developed by each, assumed a mass density less than 1 gm/cm^3. Values of density calculated from photographic and radar observations (refs. 18, 21, 22, and 23) have ranged from 0.16 gm/cm^3 to 4 gm/cm^3. In assessing the available density data, related assumptions, and calculation procedures, Whipple's opinion (that the lower densities obtained from radar observed meteor data were not reliable and the higher densities were not typical of cometary debris) was taken into consideration. From the assessment, 0.5 gm/cm^3 was chosen as the value for the mass density of meteoroids (sporadic and stream) of cometary origin.

2.4 Development of Sporadic Flux-Mass Model

The flux of sporadic meteoroids, as well as of streams and lunar ejecta, are given as a function of particle mass. The available data from photographic and radar observations and from direct flight measurements have been assessed to develop a suitable engineering model of the average cumulative sporadic flux-mass relationship. It should be noted that the cumulative flux is the integrated value of the number of particles having a mass of m or greater per square meter per second.

2.4.1 Observational Data

With due consideration of the basic photographic data (ref. 10), a flux of 3.89 X 10^{-15} particles per square meter per second for a meteoroid mass of 1 gram or greater has been chosen as a point for the model and is shown on the logarithmic plot of figure 2 as point A. The uncertainty in the meteoroid mass for this flux is subject to varied opinions and ranges from a factor of at least two to plus or minus an order of magnitude. Pending further evidence, the uncertainty is estimated as being one-fifth to five times the chosen mass.

Because of more severe selection effects for the radar technique than for the photographic technique, the radar meteor data have not been used in developing the sporadic flux-mass model. These data, however, as indicated in figure 2, do strengthen the credence in the model presented herein.

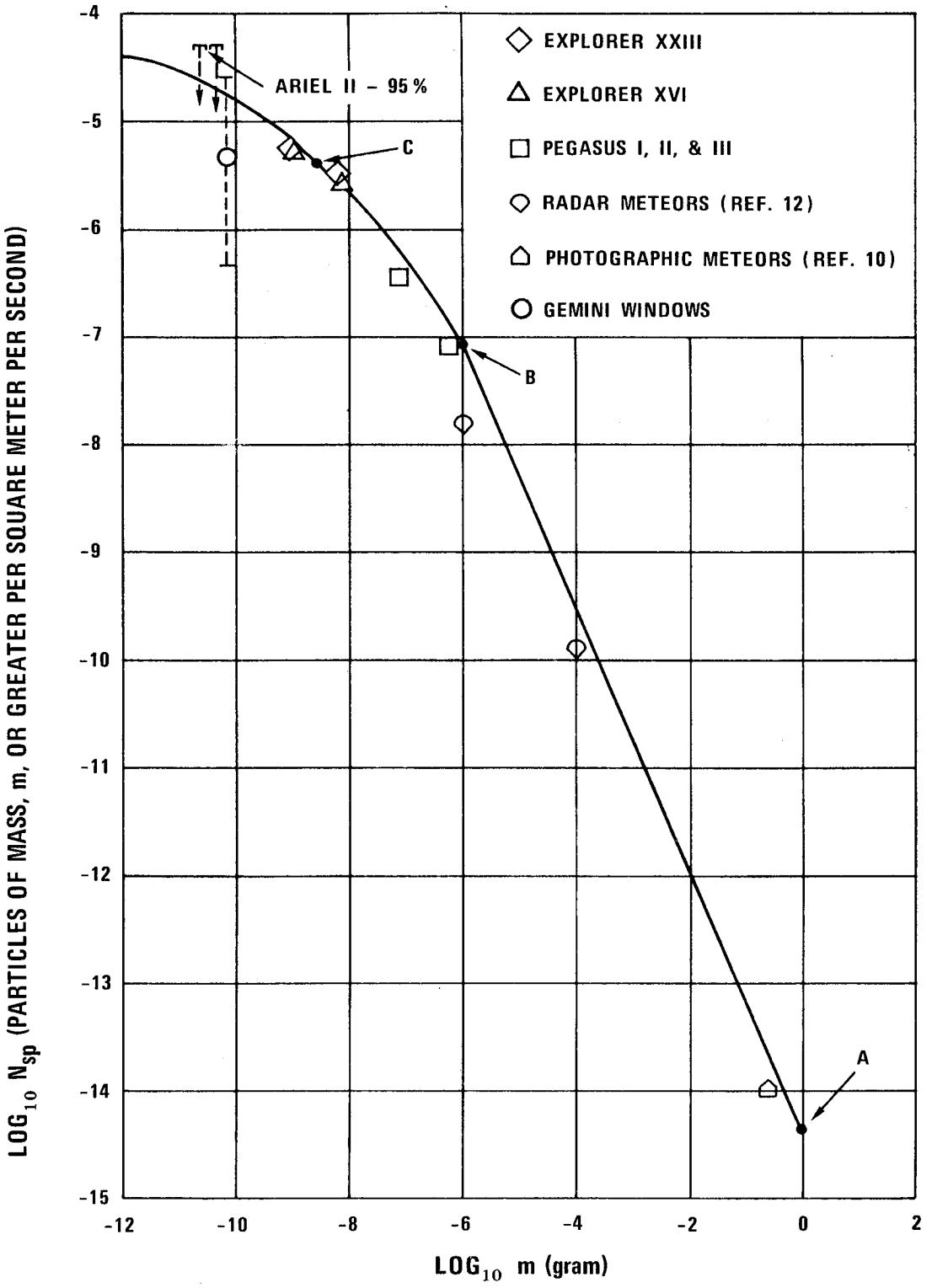

Figure 2.—Comparison of cumulative sporadic meteoroid flux-mass data and the adopted sporadic model.

2.4.2 Direct Measurement Data

In the mass range 10^{-6} gram and less, the flux-mass model has been developed from direct measurement data that were obtained as a result of pentration damage by meteoroids to instrumented spacecraft. The penetration sensor data from references 5, 6, 7, and 24 have been used to establish the sporadic flux-mass relationship in the mass range 10^{-9} to 10^{-6} gram. Conversion of the penetration data from sensor material thickness to particle mass has been accomplished by calculating the critical mass that will just perforate the sensor thickness in question. Currently, no direct experimental determination of this critical mass is possible at the average impact velocity of sporadic meteoroids. Various theoretical and empirical equations, however, such as given in references 24 and 25, have been derived by testing at hypervelocities (7.5 to 12 km/sec) and extrapolating the laboratory relationship to meteoroid velocities to obtain the critical mass.

In this monograph, an unpublished empirical equation based in part on the hypervelocity impact studies of R.H. Fish and J.L. Summers of the NASA Ames Research Center has been used to establish a characteristic meteoroid mass for threshold penetration of the sensors employed on the Pegasus and Explorer meteoroid detection satellites. The equation which is applicable to threshold penetration of single thin ductile metal plates is as follows:

$$t = K_1 \rho^{\frac{1}{6}} m^{.352} V^{.875}$$

where
- t is the thickness of the plate penetrated (cm)
- K_1 is a constant
- ρ is the mass density of the meteoroid (gm/cm^3)
- m is the mass of the meteoroid (gm)
- V is the normal impact velocity of the meteoroid (km/sec)

The constant, K_1, is a characteristic of the plate material. It reflects the combined effects of the material's strength, density, ductility, and temperature on threshold penetration as determined from hypervelocity impact tests. In applying the equation, ρ was taken as 0.5 gm/cm^3 (the chosen average mass density of meteoroids), V as 20 km/sec (the adopted average velocity of sporadic meteoroids), and K_1 as established from hypervelocity impact tests on a material. Table I presents the calculated characteristic mass for the sensors indicated, the value of K_1 for each sensor material involved, and the cumulative flux as determined from each penetration sensor system. The flux values, as presented, have not been corrected for Earth gravitational effects but have been corrected for Earth shielding effects as discussed in section 2.7.

The logarithms of the flux and mass values from table I are plotted in figure 2. Uncertainty in the directly measured flux is small (< 10%) as a result of the large number of penetrations

TABLE I

SPORADIC FLUX-MASS DATA FROM PENETRATION MEASUREMENTS

SPACECRAFT	SENSOR MATERIAL	K_1	SENSOR THICKNESS t (cm)	CHARACTERISTIC MASS m (gm)	CUMULATIVE FLUX N_{sp} (m^{-2} -sec^{-1})	LOG_{10} m (gm)	LOG_{10} N_{sp} (m^{-2} -sec^{-1})
PEGASUS I, II, III	ALUMINUM 2024 - T3	0.54	0.0406	5.20×10^{-7}	8.00×10^{-8}	-6.28	-7.10
			0.0203	7.25×10^{-8}	3.44×10^{-7}	-7.14	-6.46
EXPLORER XXIII	STAINLESS STEEL TYPE 302	0.32	0.0051	6.29×10^{-9}	3.33×10^{-6}	-8.20	-5.48
			0.0025	8.28×10^{-10}	5.68×10^{-6}	-9.08	-5.25
EXPLORER XVI	BERYLLIUM COPPER	0.30	0.0051	7.55×10^{-9}	2.66×10^{-6}	-8.12	-5.58
	BERYLCO NO. 25		0.0025	9.95×10^{-10}	5.16×10^{-6}	-9.00	-5.29

obtained on each sensor system. The characteristic mass for threshold penetration as calculated for each sensor is probably correct within a factor of three (3) even though there is some evidence that the equation may underestimate the threshold penetration mass in the plate thickness range of the sensors employed.

The data from the 0.0406 cm sensor on Pegasus II and III have been used to establish another point for the model. A cumulative flux of 8.00×10^{-8} particles per square meter per second for a mass of $10^{-6.0}$ gram or greater was adopted (point B in fig. 2). The conservative selection of the $10^{-6.0}$ gram mass rather than a $10^{-6.28}$ gram mass as calculated (table I) was chosen because of the indications of ballistic limit data obtained from hypervelocity impact tests on the actual 0.0406 cm Pegasus sensor. These unpublished data extrapolated to the average velocity for sporadic meteoroids (20 km/sec) indicate that the sensor as shown has a characteristic mass for threshold penetration between $10^{-6.0}$ gram and $10^{-5.8}$ gram.

The data from Explorer XVI and XXIII are considered to be the most reliable and, as shown in figure 2, are consistent in showing a decrease in the slope of the flux-mass relationship in the mass range 10^{-9} to 10^{-8} gram. Assuming the adopted flux at 10^{-6} gram is reliable, the decrease in slope is in agreement with the evidence provided by the intensity of zodiacal light and the concept of a physical limit to the amount of particulate debris in the solar system. Further indication of the slope trend is provided by the Ariel II results (ref. 26) and unpublished results stemming from postflight examination of fourteen Gemini spacecraft windows (fig. 2). Accordingly, the Explorer data points have been used to determine the shape of the flux-mass curve at masses less than 10^{-6} gram.

2.4.3 Summary of Model Development

In the mass range 10^{-6} gram and greater (points A to B in fig. 2), a straight line variation has been assumed; in the range 10^{-6} gram and less, where the penetration data indicated a decrease in the slope of the flux-mass relationship with decreasing mass, a nonlinear variation passing through the Explorer data has been adopted between 10^{-6} to 10^{-12} gram. At the latter mass, the model was arbitrarily terminated. A cumulative flux of 3.98×10^{-6} particles per square meter per second together with a mass of 2.5×10^{-9} gram (point C in fig. 2) was chosen to give a best fit to all four of the Explorer data points in determining an equation for the nonlinear variation. The model along with the applicable mathematical equations is shown in figure 3. The fluxes are gravitationally focused unshielded values.

In the development of the particular sporadic flux-mass model presented, consideration was given to other models derived by Whipple (ref. 9), Naumann (ref. 24), Dalton (ref. 27), Dohnanyi (ref. 16), and the Apollo design environment (ref. 28) and the NASA Manned Spacecraft Center design environment (ref. 29). Three of these models, and the model developed herein, are shown in figure 4 for comparative purposes.

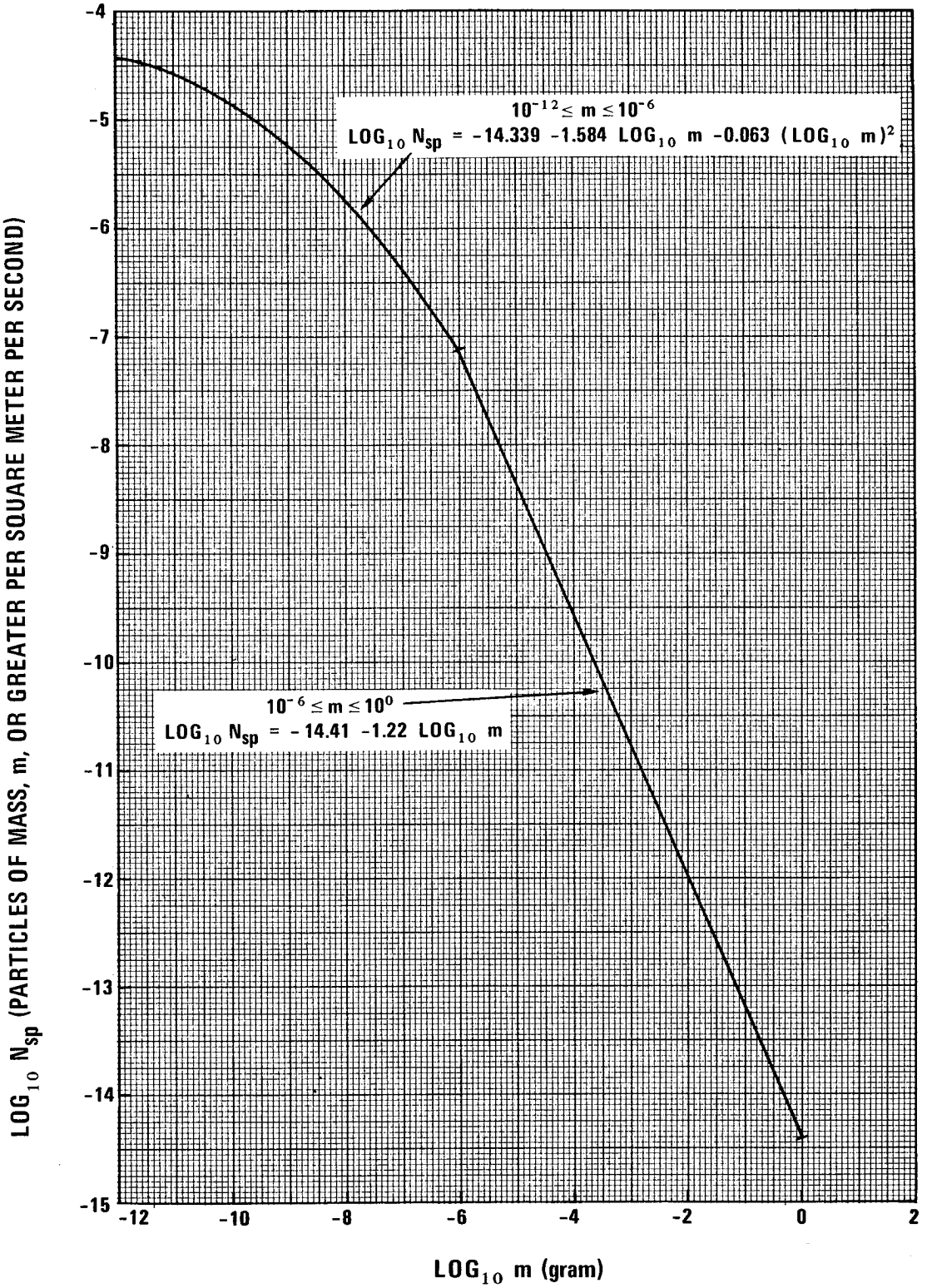

Figure 3.—Average cumulative sporadic meteoroid flux-mass model for 1 A.U.

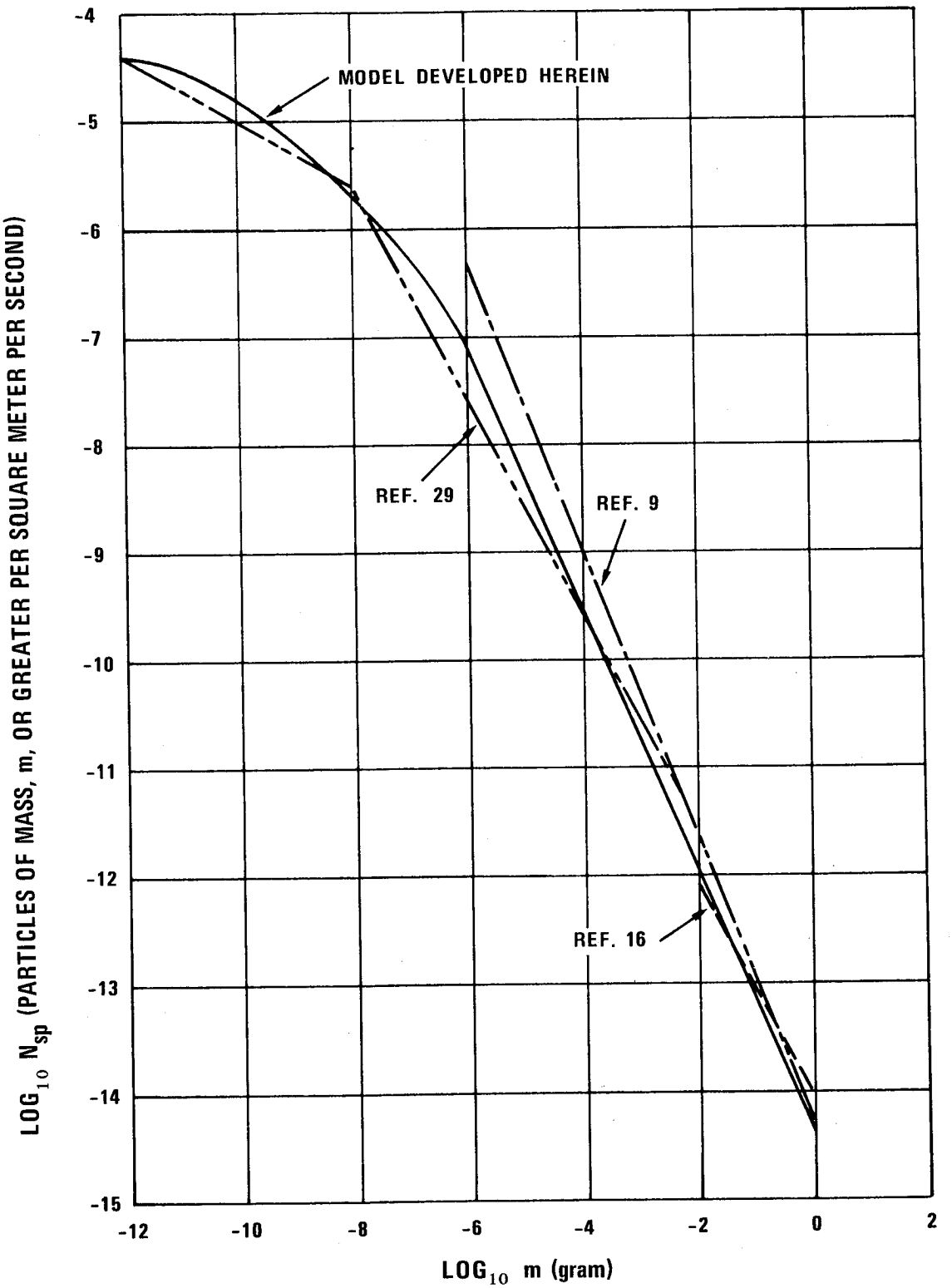

Figure 4.–Comparison of sporadic flux-mass models.

2.5 Development of Stream Flux-Mass Model

Noticeable increases in the average hourly rate of meteor activity have been observed at regular intervals during the calendar year. These increases are caused by the Earth's passage through a stream of particles traveling in similar heliocentric orbits. In this monograph the particles have been assumed to be of cometary origin. This assumption is supported by the definite association of a large number of the individual streams with comet orbits. The orbital elements, velocity, and periods of occurrence of eighteen of the more prominent streams, as given in reference 19, are listed in table II and the orbital elements are defined in figure 5.

Observations of meteor activity by the photographic and radar techniques have been made by a number of investigators (refs. 1, 11, and 30) to obtain the influx rate of stream meteoroids. The approximate mass range of stream particles covered by the photographic and radar techniques is 10^{-1} to 1 gram and 10^{-4} to 10^{-2} gram, respectively. These observations have indicated that there are increases in the total meteoroid flux during a period of stream activity in the photographic mass range, but the portion attributed to a stream tended to decrease with decreasing mass. In the radar mass range, the stream activity was found to be below the sporadic activity with a few exceptions (ref. 11) such as the Perseids and the Leonids. Since the observational data on the stream activity involves the sporadic flux, the flux of each stream from the observational data has been described in reference 19 as the ratio, F, of the cumulative flux of each stream to the average cumulative sporadic flux. These activity ratios as developed in reference 29 from photographic data on meteors with masses equal to or greater than 10^{-1} gram are given in figure 6 as functions of time within each stream's duration and are used in the mathematical description of the flux-mass relationship of each individual stream. These activity ratio distributions are idealized representations of the actual flux-time variation of the streams and are for engineering application only.

Because of the paucity of flux-mass information for individual streams, the stream flux-mass relationship is assumed to be similar to that of the sporadic activity in the mass range 10^{-6} gm $\leq$ m $\leq$ 1 gm. Accordingly, the flux-mass expression from reference 29, which accounts for the stream's activity ratio and average geocentric velocity, has been adopted as the model applicable to each individual stream. The expression, however, has been modified to reflect the 20 km/sec average velocity of sporadics and the log of the sporadic flux constant in the mass range 10^{-6} gm $\leq$ m $\leq$ 1 gm. The model allows each stream to "vanish" into the background sporadic activity at differing masses and is applicable in the mass range 10^{-6} gm $\leq$ m $\leq$ 1 gm. Also in the absence of more precise data, the activity ratios shown in figure 6 for a mass, m $\leq 10^{-1}$ gm have been assumed to be the applicable values of F for a stream particle mass of 1 gm and greater with a velocity of 20 km/sec. In the model expression, the use of an integrated average value of F for a shower gives an average cumulative flux-mass relationship for the period of the duration desired. Correspondingly, a maximum value of F, as given in table II, indicates the shower contribution during the peak activity.

TABLE II

MAJOR METEOROID STREAMS

Name	Period of activity	Date of maximum	F_{max} (a)	Orbital elements (defined in fig.5)							Velocity
				Ω, deg.	π, deg.	ω, deg.	ι, deg.	ϵ	q, A. U.	a, A. U.	Geocentric, km/sec
Quadrantids	Jan. 2 to 4	Jan. 3	8.0	282	92	166	67	0.46	0.97	1.7	42
Lyrids	Apr. 19 to 22	Apr. 21	0.85	30.5	--	210	81	0.88	0.90	--	48
η - Aquarids	May 1 to 8	May 4 to 6	2.2	45	152	108	162	0.96	0.66	17.95	64
o - Cetids	May 14 to 23	May 14 to 23	2.0	238	89	211	34	0.91	0.11	1.3	37
Arietids	May 29 to June 19	June 6	4.5	77	106	29	21	0.94	0.09	1.6	38
ζ - Perseids	June 1 to 16	June 6	3.0	78	--	59	4±2	0.79	0.35	1.6	29
β - Taurids	June 24 to July 5	June 28	2.0	276	162±4	246±4	9±4	0.86	0.36	2.5	31
δ - Aquarids	July 26 to Aug. 5	July 28	1.5	305	101±2	156±2	24±5	0.96	0.08	1.8	40
Perseids	July 15 to Aug. 18	Aug. 10 to 14	5.0	142	--	155	114	0.96	0.97	23	60
Orionids	Oct. 15 to 25	Oct. 20 to 23	1.2	29.3	103	87.8	163	0.92	0.54	6.32	66
Arietids, southern	Oct.1 to Nov.28	Nov. 5	1.1	27	150	122	6	0.85	0.30	1.91	28
Taurids, northern	Oct. 26 to Nov. 22	Nov. 10	0.4	221	160	308	2.5	0.86	0.31	2.16	29
Taurids, night	Nov.1 to Nov.30	Nov.15	1.0	220	160	300	3	0.86	0.3	2.1	37
Taurids, southern	Oct. 26 to Nov. 22	Nov. 5	0.9	45	157	112	5.1	0.85	0.36	2.39	28
Leonids southern	Nov. 15 to 20	Nov. 16 to 17	0.9	234	49	179	162	0.92	0.99	12.8	72
Bielids	Nov. 12 to 16	Nov. 14	0.4	250	109	223	13	0.76	0.88	3.6	16
Geminids	Nov. 25 to Dec. 17	Dec. 12 to 13	4.0	261	--	324	24	0.90	0.14	1.4	35
Ursids	Dec. 20 to 24	Dec. 22	2.5	270	--	210	56 ±3	1.0	0.92	--	37

(a) F_{max} = Ratio of maximum cumulative flux of stream to average cumulative sporadic flux

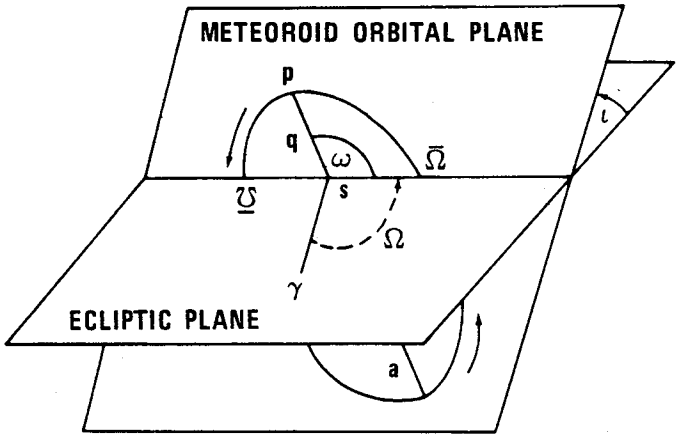

a = SEMI - MAJOR AXIS, A. U.
p = POINT OF PERIHELION
q = PERIHELION DISTANCE, A. U.
S = SUN
γ = HELIOCENTRIC DIRECTION OF THE VERNAL EQUINOX
ι = INCLINATION OF METEROID ORBITAL PLANE, DEG
ω = ARGUMENT OF PERILELION, DEG
$\pi = \Omega + \omega$
Ω = LONGITUDE OF ASCENDING NODE, DEG.
$\overline{\Omega}$ = ASCENDING NODE
$\underline{\Omega}$ = DESCENDING NODE

Orbital Elements

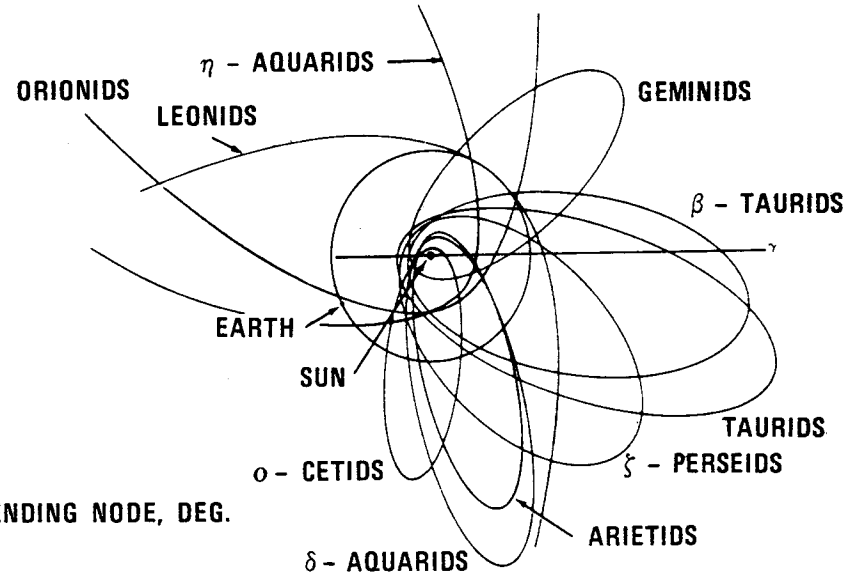

Selected Orbits Intersecting Earth Orbit

Figure 5.–Meteoroid stream orbital elements and selected orbits.

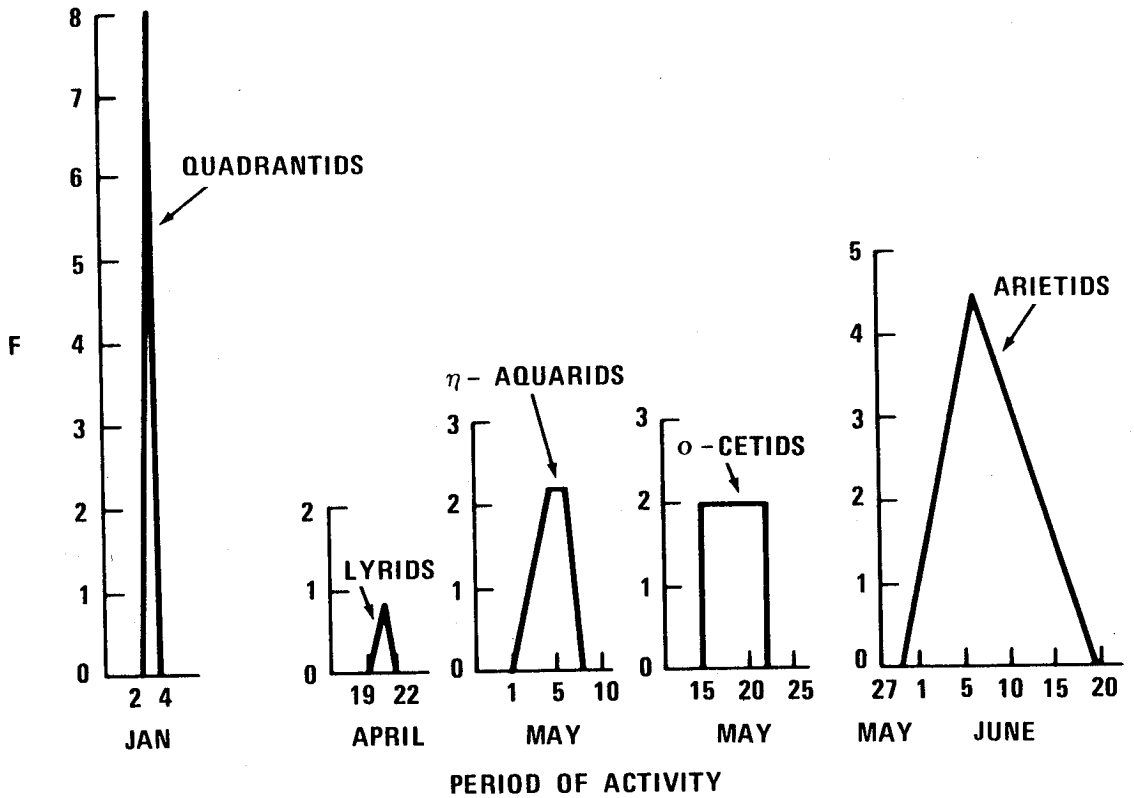

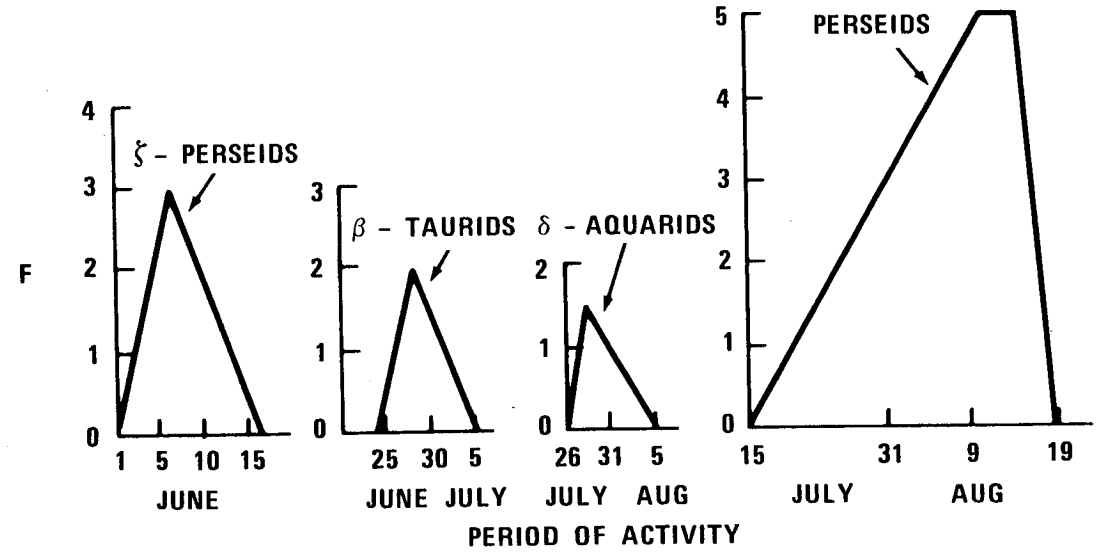

$$F = \frac{\text{CUMULATIVE FLUX OF STREAM}}{\text{AVERAGE CUMULATIVE SPORADIC FLUX}}$$

Figure 6a.—Activity ratio factor versus period of activity (January-August) for major streams based on photographic meteors with mass, $m \geq 10^{-1}$ gram.

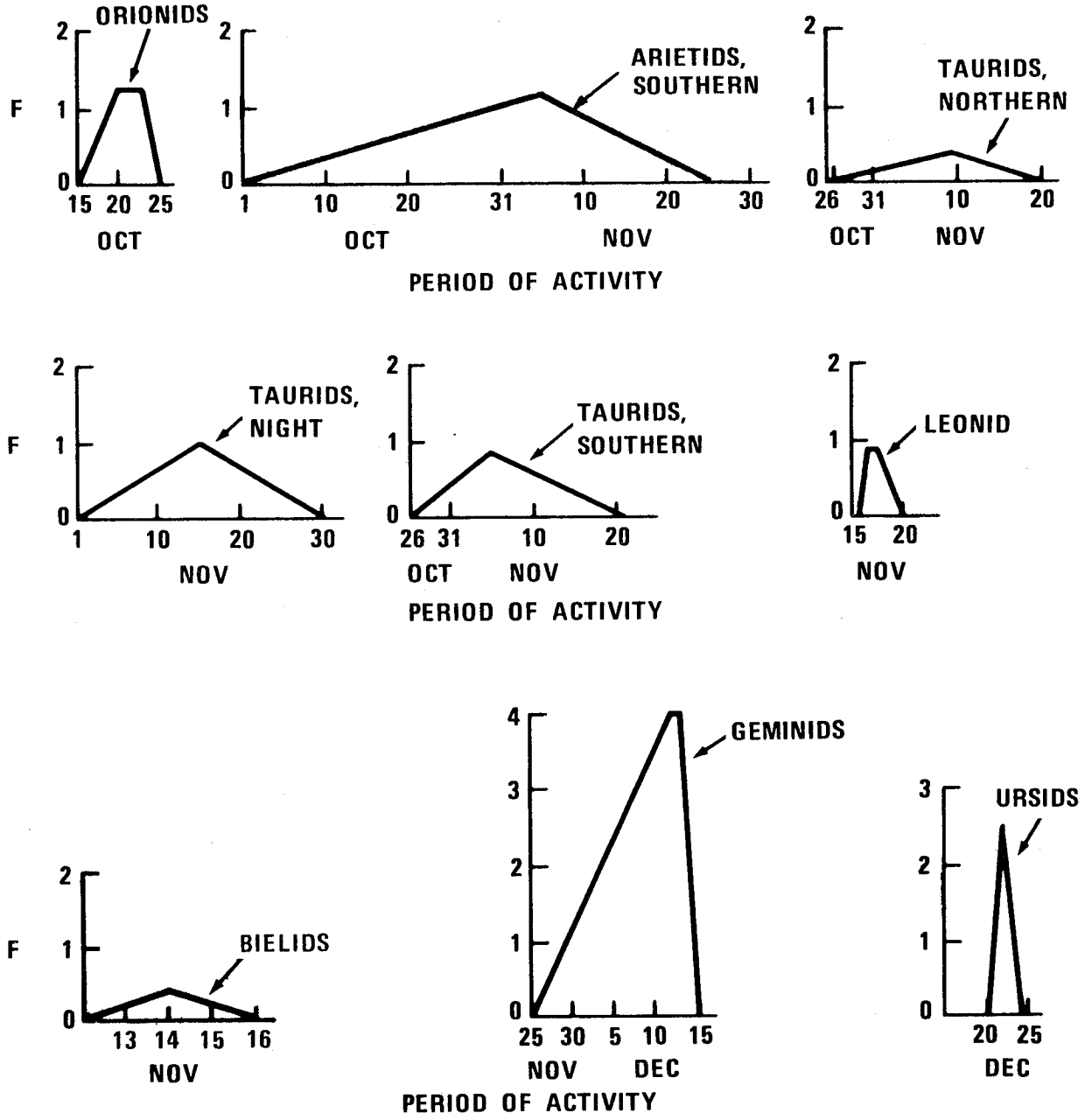

Figure 6b.—Activity ratio factor versus period of activity (September-December) for major streams based on photographic meteors with mass, $m \geq 10^{-1}$ gram.

It should be noted that the stream flux-mass relationship is only applicable in design to a vehicle with a rigidly specified mission period. The relationship, however, does provide a basis for evaluating specific stream damage to a vehicle designed for an unspecified mission period.

2.6 Development of a Total Meteoroid Flux-Mass Model

For use in preliminary design and where launch date and mission duration are not specified, an average cumulative total meteoroid (average sporadic plus average stream) flux-mass model is needed to consider the meteoroid hazard. Such a model has been developed by modifying the sporadic model (sec. 2.4) to account for the stream activity shown in figure 6 and the decreasing stream activity with decreasing mass noted in the radar data (sec. 2.5). To account for the average stream activity, an average annual value of the activity ratio, F, equal to 0.1 has been used, based on a constant mass approach. The calculated value from the accumulated ratios of the streams over the calendar year is slightly less than the value used. As in the case for specific streams (sec. 2.5), the 10% increase in average flux due to streams was assumed to be applicable to a meteoroid particle mass of 1 gram with a 20 km/sec velocity. Accordingly, the derived mathematical expression starts with a cumulative total meteoroid flux of 1.1 times the sporadic at m = 1 gm and allows the stream component to "vanish" into the sporadic at approximately m = 10^{-6} gm. The total meteoroid flux-mass model is shown in figure 7.

2.7 Gravitational and Body Shielding Factors

There are two phenomena which influence the actual flux encountered by spacecraft in near-Earth, cislunar, and lunar missions. These phenomena are the gravitational and shielding effects of the Earth and the Moon.

Whipple (ref. 9) has calculated the differences in the cometary meteoroid environment near the Earth and on the Moon. Dohnanyi (ref. 16) and Hale and Wright (ref. 31) have also calculated the decrease in flux with distance from the Earth. Thus the flux, particularly that of the slower moving meteoroids, that has been obtained by the Earth-based observational techniques and orbital direct measurements is assumed to have been enhanced by Earth's gravity; i.e., the sporadic flux model is gravitationally focused. The actual number of meteoroid impacts encountered by a spacecraft is also influenced by its orbital altitude above a shielding body. The Earth and Moon may act as shields to reduce the impacts of sporadic meteoroids and to block the impacts of stream meteoroids when the orbital tracks of the spacecraft, Earth or Moon, and a stream are so aligned.

To correct for the the Earth's gravitational enhancement at a given distance above the Earth, the average sporadic (sec. 2.4) or total meteoroid flux (sec. 2.6) must be multiplied by the defocusing factor, G_e, adopted from reference 32. The factor, G_e, as a function of distance above the center of the Earth in Earth radii is given in figure 8.

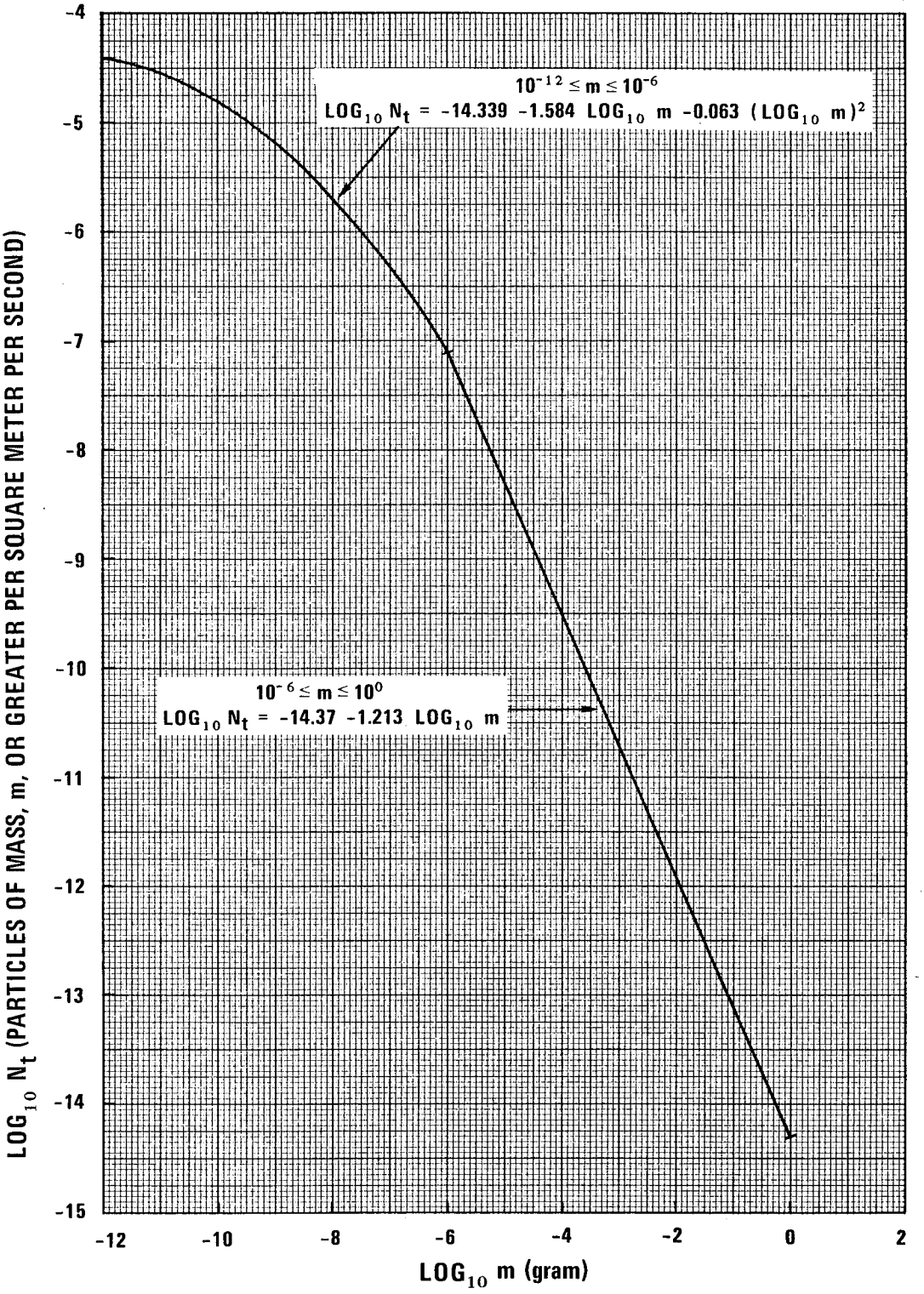

Figure 7.—Average cumulative total meteoroid flux-mass model for 1 A.U.

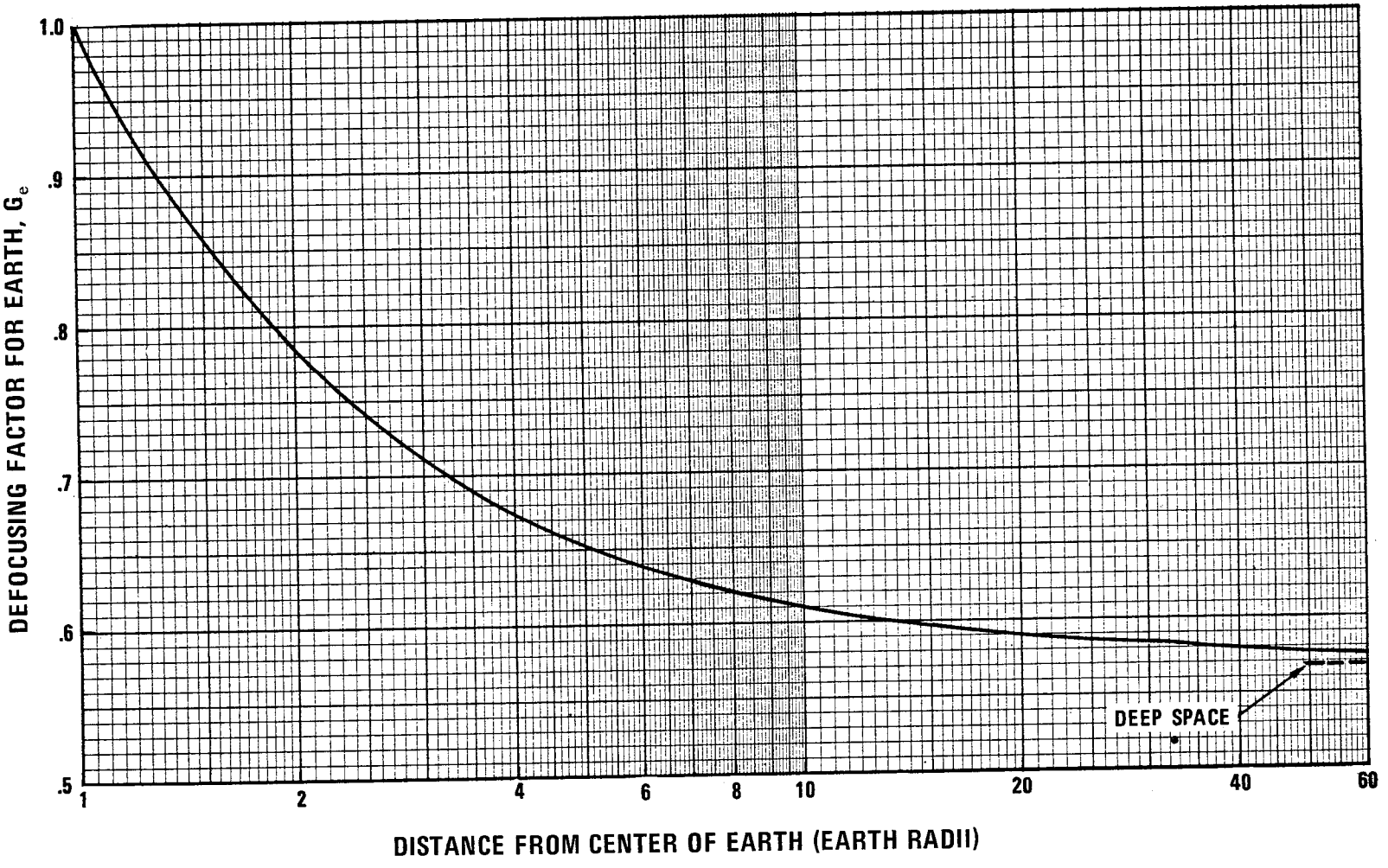

Figure 8.–Defocusing factor due to Earth's gravity for average meteoroid velocity of 20 km/sec.

The gravitational effect of the Earth and Moon on the flux of stream meteoroids, because of their higher velocities, has been assumed to be negligible and has been omitted.

The number of impacts as seen by a spacecraft shielded by the Earth or Moon or as seen by a spacecraft component shielded by the spacecraft is a function of the spacecraft or component shape and its orientation with respect to the shielding body. If the spacecraft is spherically shaped and randomly oriented, the actual number of impacts can be treated as the product of the unshielded defocused flux and the shielding factor, ζ, as defined in figure 9 for the Earth or the Moon. Multiplying by the factor, ζ, has the effect of subtracting out the flux within the solid angle subtended by the shielding body (fig. 9). Although based on a spherical spacecraft, the factor, ζ, will produce only a small error in the actual average sporadic or total meteoroid flux impacting on a spacecraft of any shape provided the spacecraft is randomly oriented. For oriented spacecraft, body shielding effects have to be considered on an individual design basis as the shielding affects only the side toward the shielding body. Similarly, body shielding effects applicable to stream meteoroids have to be determined on an individual basis.

2.8 Lunar Surface Ejecta

It has been postulated that meteoroid impacts on the lunar surface will eject material that will create an additional hazard in the rarefied lunar atmosphere up to an altitude of 30 km. Such lunar ejecta, because of their relative low velocity as compared to meteoroids, are predominately a hazard in extravehicular activities and other operations on or near the lunar surface.

Laboratory experiments involving hypervelocity impacts into basalt and weakly bonded sand (ref. 33) have indicated that this flux is approximately 10^4 times larger than the meteoroid flux. Additional experiments (ref. 34) with dendritic structures of bonded sands and pumice have shown that such ejecta exist for these structures and materials. The ejecta flux was found to be 10^3 times the impacting flux for a sand of 70% porosity and were reduced significantly only when the impacted material was pumice (40 times the primary). Zook (ref. 35) has derived an expression for determining the ejecta flux-mass relationship according to velocity intervals of the ejected particles. Most of the ejecta were shown to be traveling at velocities under 1 km/sec. This particular form for the mass and velocity distribution of lunar ejecta has been adopted and a cumulative lunar ejecta flux-mass model for ejecta velocity intervals of 0-0.1, 0.1-0.25, and 0.25-1.0 km/sec has been determined, utilizing the average sporadic flux-mass model presented in this monograph. This ejecta flux-mass relationship is shown in figure 10 and, although not based on a total meteoroid flux-mass model, is adequate for considering the postulated ejecta particles.

Similarly, an average cumulative mass-flux distribution for the total lunar ejecta ($0 \leq V_e \leq 1.00$ km/sec) has been determined. This average distribution along with an average lunar ejecta velocity of 0.1 km/sec has application primarily in preliminary design.

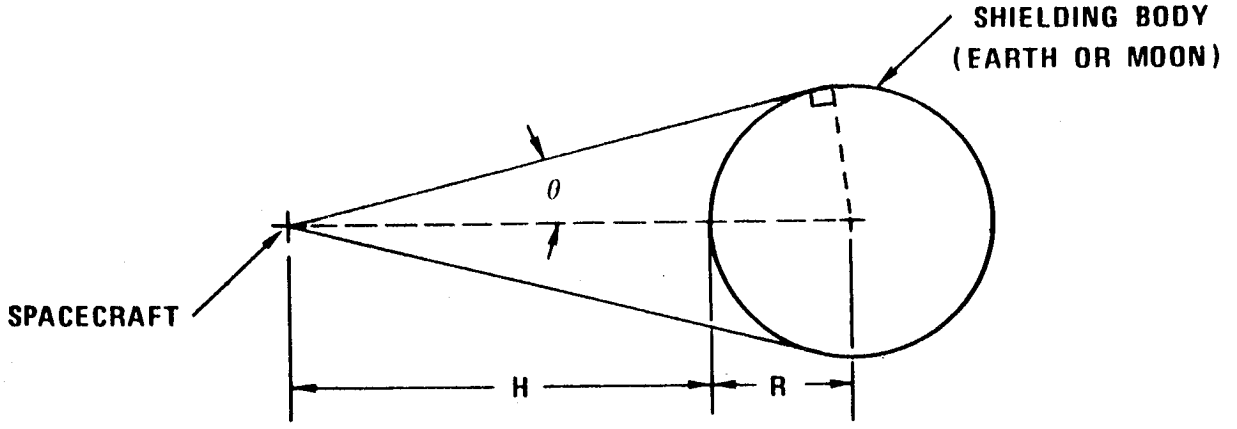

BODY SHIELDING FACTOR, ζ : (Defined as ratio of the shielded to unshielded flux)

$$\zeta = \frac{1 + \cos\theta}{2}$$

WHERE:

$$\sin\theta = \frac{R}{R + H}$$

R Radius of Shielding Body
H Altitude above Surface

Subscripts:
e Earth
m Moon

Figure 9.—Method for determining body shielding factor for randomly oriented spacecraft.

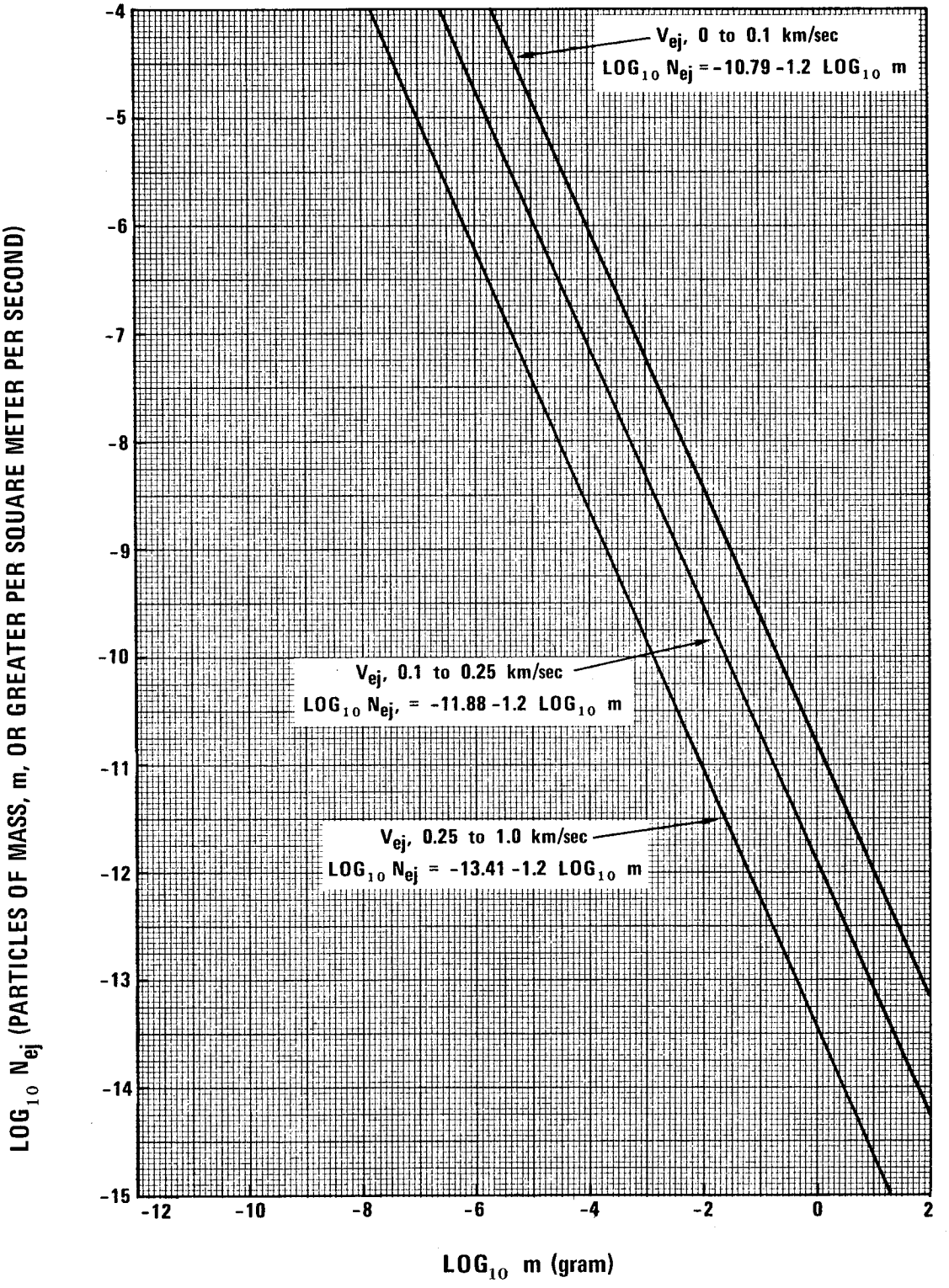

Figure 10.–Average cumulative lunar ejecta flux-mass distribution for each of three ejecta velocity intervals.

On the basis that the lunar surface is composed of a basalt type (volcanic) material, a mass density of 2.5 gm/cm^3 has been adopted for the ejecta created by the impacting meteoroid particles.

3. CRITERIA

The meteoroid and lunar ejecta flux-mass models and the associated particle density and velocity values presented in the following subsections should be used to establish the meteoroid environment for engineering application to space missions in near-Earth orbit, cislunar space, lunar orbit, and on the lunar surface.

3.1 Meteoroid Environment

The meteoroid environment model encompasses only particles of cometary origin and is composed of sporadic meteoroids in the mass range between 10^{-12} and 1 gram and stream meteoroids in the mass range from 10^{-6} to 1 gram.

3.1.1 Average Total Meteoroid Environment

The average total meteoroid (average sporadic plus a derived average stream) environment is to be used for preliminary design and for mission periods that cannot be specified. When the mission launch date and duration are specified later in the design, the probability of stream damage should be evaluated (sec. 3.1.3).

3.1.1.1 Particle Density

The mass density is 0.5 gm/cm^3 for all meteoroid sizes.

3.1.1.2 Particle Velocity

The average meteoroid velocity is 20 km/sec with a probability-velocity distribution as given in figure 1.

3.1.1.3 Flux-Mass Model

The average cumulative meteoroid flux-mass model is shown in logarithmic form in figure 7 and is described mathematically as follows:

$10^{-6} \leq m \leq 10^{0}$ $\quad \text{Log}_{10} N_t = -14.37 \ -1.213 \ \log_{10} m$

$10^{-12} \leq m \leq 10^{-6}$ $\quad \text{Log}_{10} N_t = -14.339 - 1.584 \ \log_{10} m \ -0.063 \ (\log_{10} m)^2$

where

N_t = number of particles of mass m or greater per square meter per second*
m = particle mass in grams

The gravitationally focused, unshielded flux, N_t, must be multiplied by an appropriate defocusing factor for Earth, G_e, and, if applicable, by the shielding factor (sec. 2.7). The G_e factor applies to all missions and is to be obtained from figure 8. The body shielding factor for randomly oriented spacecraft, ζ, is calculated by the method given in figure 9 and applies to all missions. For oriented spacecraft, the effects of body shielding on the number of impacts as seen by parts of the spacecraft must be determined on an unique basis.

3.1.2 Sporadic Meteoroids

The average sporadic meteoroid environment is to be used in conjunction with the specific stream meteoroid environment (sec. 3.1.3) in design of a vehicle with a specified mission period (launch date and duration).

3.1.2.1 Particle Density

The mass density is 0.5 gm/cm^3 for all sporadic particle sizes.

3.1.2.2 Particle Velocity

The average sporadic particle velocity is 20 km/sec with a probability-velocity distribution as given in figure 1.

*Log_{10} N (particles/ft^2/day) = Log_{10} N (particles/m^2/sec) + 3.906

3.1.2.3 Flux-Mass Model

The average cumulative sporadic flux-mass model is shown in logarithmic form in figure 3 and is described mathematically as follows:

$10^{-6} \leq m \leq 10^{0}$ $\quad\quad$ $\text{Log}_{10} N_{sp} = -14.41 \ -1.22 \ \log_{10} m$

$10^{-12} \leq m \leq 10^{-6}$ $\quad\quad$ $\text{Log}_{10} N_{sp} = -14.339 - 1.584 \log_{10} m - 0.063 (\log_{10} m)^2$

where

N_{sp} = number of sporadic particles of mass m or greater per square meter per second
m = particle mass in grams

The gravitationally focused unshielded flux, N_{sp}, must be multiplied by an appropriate defocusing factor for the Earth, G_e, and, if applicable, by the shielding factor (sec. 2.7). The G_e factor applies to all missions and is to be obtained from figure 8. The body shielding factor for randomly oriented spacecraft, ζ, is calculated by the method given in figure 9 and applies to all missions. For oriented spacecraft, the effects of body shielding on the number of impacts as seen by parts of a spacecraft must be determined on a unique basis.

3.1.3 Stream Meteoroids

The specific stream environment is to be used in the design of a vehicle with a specified mission period (launch date and duration) and as a means of determining the probability of stream damage to a spacecraft that has been designed to an average annual total meteoroid environment.

3.1.3.1 Particle Density

The mass density is 0.5 gm/cm^3 for all stream particle sizes.

3.1.3.2 Particle Velocity

The particle velocity of each stream is that given in table II.

3.1.3.3 Flux-Mass Model

The cumulative flux-mass model applicable to each individual stream is described mathematically as follows:

$$10^{-6} \leq m \leq 10^{0} \qquad \text{Log}_{10}\ N_{st} = -14.41 - \log_{10} m - 4.0 \log_{10}\left(\frac{V_{st}}{20}\right) + \log_{10} F$$

where

N_{st} = number of stream particles of mass m or greater per square meter per second
m = particle mass in grams
V_{st} = geocentric velocity of each stream in km/sec from table II
F = integrated average ratio of cumulative flux of stream to the average cumulative sporadic flux as calculated from figure 6 for the portion of the stream's duration within the mission period.

No gravitational factor is to be applied to the flux of a specific stream. Similarly, there is no shielding effect unless a shielding body eclipses the spacecraft relative to the radiant of a stream as given in table I. When an eclipse occurs, the flux of that specific stream is zero.

3.2 Lunar Ejecta Environment

The lunar ejecta environment encompasses the lunar particles ejected from impacts of meteoroids on the lunar surface. In addition to the hazard of meteoroids in extravehicular activities and other operations on or near the lunar surface, lunar ejecta must be considered. The lunar ejecta environment given herein is to be used from the lunar surface to an altitude of 30 km. The effects of the ejecta environment must be considered separately from meteoroids because of their different velocity regimes.

3.2.1 Particle Density

The mass density is 2.5 gm/cm^3 for all ejecta particle sizes.

3.2.2 Particle Velocity

The average ejecta velocity is 0.1 km/sec for all ejecta particle sizes.

3.2.3 Flux-Mass Models

3.2.3.1 Average Total Ejecta Flux-Mass Model

An average annual total cumulative flux-mass model for the lunar ejecta is to be used in preliminary design and is described as follows:

$0 \leq V_{ej} \leq 1.0$ $\qquad$ $\text{Log}_{10} N_{ej_t} = -10.75 - 1.2 \log_{10} m$

where

N_{ej_t} = number of ejecta particles of mass m or greater per square meter per second
m = particle mass in grams

The average ejecta velocity, 0.1 km/sec, is to be used with this distribution model.

3.2.3.2 Individual Ejecta Flux-Mass Models

An average annual individual cumulative lunar ejecta flux-mass distribution for each of three velocity intervals should be used in detailed consideration of the ejecta hazard. These three distributions and the corresponding adopted ejecta velocity for each distribution are:

$0 \leq V_{ej} \leq 0.1$ $\qquad$ $\text{Log}_{10} N_{ej} = -10.79 - 1.2 \log_{10} m$

$V_{ej} = 0.1$ km/sec

$0.1 \leq V_{ej} \leq 0.25$ $\qquad$ $\text{Log}_{10} N_{ej} = -11.88 - 1.2 \log_{10} m$

$V_{ej} = 0.25$ km/sec

$0.25 \leq V_{ej} \leq 1.0$ $\qquad$ $\text{Log}_{10} N_{ej} = -13.41 - 1.2 \log_{10} m$

$V_{ej} = 1.0$ km/sec

REFERENCES

1. Lovell, A. C.: Meteor Astronomy. Oxford University Press, 1954.

2. McKinley, D. W.: Meteor Science and Engineering. McGraw-Hill Book Company, Inc., 1961.

3. Watson, F. G.: Between the Planets. Harvard University Press, 1956.

4. Alexander, W. M.; McCracken, C. W.; Secretan, L.; and Berg, O.: Review of Direct Measurements of Interplanetary Dust from Satellites and Probes. Space Research III; Proceedings of the Third International Space Science Symposium, Woflgang Priester, ed., John Wiley and Sons, Inc., 1963, pp. 891-917.

5. Hastings, E. C.: The Explorer XVI Micrometeoroid Satellite Supplement III, Preliminary Results for Period May 27, 1963 through July 22, 1963. NASA TMX-949, March 1964.

6. O'Neal, R. L.: The Explorer XXIII Micrometeoroid Satellite. NASA TN D-4284, June 1968.

7. Clifton, S.; and Nauman, R.: Pegasus Satellite Measurements of Meteoroid Penetration (Feb. 16-Dec. 31, 1965). NASA TMX 1316, December 1966.

8. Hawkins, G. S.; and Upton, E. K.: The Influx Rate of Meteors in the Earth's Atmosphere. Astrophysical Journal, vol. 128, 1958, pp. 727-735.

9. Whipple, F. L.: The Meteoritic Environment of the Moon. Royal Society (London), Proceedings, Series A, vol. 296, Feb. 7, 1967, pp. 304-315.

10. Lindblad, B. A.: The Luminosity Function of Sporadic Meteors and the Extrapolation of the Meteor Influx Rate to the Micrometeorite Region. The Proceedings of a Symposium on Meteor Orbits and Dust, NASA SP-135, 1967, pp. 171-180.

11. Elford, W. G.: The Incidence of Meteors on the Earth Derived from Radio Observations. The Proceedings of a Symposium on Meteor Orbits and Dust, NASA SP-135, 1967, pp. 121-132.

12. Nilsson, C. S.; and Southworth, R. B.: The Flux of Meteors and Micrometeoroids in the Neighborhood of the Earth. Smithsonian Astrophysical Observatory Special Report No. 263, December 1967.

13. Kashcheyev, B. L.; and Lebedinets, V. N.: Radar Studies of Meteors. The Proceedings of a Symposium on Meteor Orbits and Dust, NASA SP-135, 1967, pp. 183-199.

14. McCrosky, R. E.; and Posen, A.: Orbital Elements of Photographic Meteors. Smithsonian Contributions to Astrophysics 4, no. 2, 1961 pp 15-84.

15. Hawkins, G. S.; and Southworth, R. B.: The Statistics of Meteors in the Earth's Atmosphere. Smithsonian Contributions to Astrophysics 2, 1958, pp. 349-364.

16. Dohnanyi, J. S.: Model Distribution of Photographic Meteors. Bellcomm, Inc. Report TR-66-34-1, 1966.

17. Dalton, C. C.: Statistical Analysis of Photographic Meteor Data, Part II: Verniani's Luminous Efficiency and Supplemented Whipple Weighting. NASA TMX-53360, November 1965.

18. Whipple, F. L.: On Meteoroids and Penetration. Journal of Geophysical Research, vol. 68, no. 17, 1963, pp. 4929-4939.

19. Burbank, P. B.; Cour-Palais, B. G.; and McAllum, W. E.: A Meteoroid Environment for Near-Earth, Cislunar and Near-Lunar Operations. NASA TN D-2747, April 1965.

20. Whipple, F. L.: The Meteoritic Risk to Space Vehicles, Vistas in Astronautics, Pergammon Press, Los Angeles, 1958.

21. Verniani, F.: On the Luminous Efficiency of Meteors. Research in Space Sciences. Smithsonian Astrophysical Observatory Special Report No. 145, 1964.

22. Verniani, F.: II Nuovo Cimento, vol. 33, no. 4, August 1964, pp. 4453-4464.

23. Ceplecha, Z.: Classification of Meteor Orbits. The Proceedings of a Symposium on Meteor Orbits and Dust, NASA SP-135, 1967, pp. 35-60.

24. Naumann, R. J.: The Near-Earth Meteoroid Environment. NASA TN D-3717, November 1966.

25. Fish, R. H.; and Summers, J. L.: The Effect of Material Properties on Threshold Penetration. Proceedings of Seventh Hypervelocity Symposium, vol. VI, February 1965.

26. Jennison, R. C.; McDonnell, J.A.M.; and Rodgers, I.: The Ariel II Micrometeorite Penetration Measurements. Proceedings of the Royal Society, vol. 300, August 1967, pp. 251-269.

27. Dalton, C. C.: Effects of Recent NASA-ARC Hypervelocity Impact Results on Meteoroid Flux and Puncture Models. NASA TMX-53512, September 1966.

28. Natural Environment and Physical Standards for the Apollo Program. NASA Office of Manned Space Flight, M-DE 8020.008B, April 1965.

29. Manned Spacecraft Center Design Specification DS-21, Rev. A, January 1967.

30. Whipple, F. L.; and Jacchia, L. G.: Precision Orbits of 413 Photographic Meteors. Smithsonian Contributions to Astrophysics 4, no. 4, 1961.

31. Hale, D. P.; and Wright, J. J.: Meteoric Flux and Density Fields about a Finite Attractive Center Generated by a Stream Monoenergetic and Monodirectional at Infinity. Journal of Geophysical Research, vol. 69, no. 17, September 1964, pp. 3719-3726.

32. Öpik, E. J.: Collision Probabilities with Planets and the Distribution of Interplanetary Matter. Proceedings of Royal Irish Academy, vol. 54, section A, April 1951, pp. 165-199.

33. Gault, D. E.; Shoemaker, E. M.; and Moore, H. J.: Spray Ejected from the Lunar Surface by Meteoroid Impact. NASA TN D-1767, April 1963.

34. Gault, D. E.; Heitowit, E. D.; and Moore, H. J.: Some Observations of Hypervelocity Impacts with Porous Media. NASA TMX-54009, December 1963.

35. Zook, H. A.: The Problem of Secondary Ejecta Near the Lunar Surface. Transactions of 1967 National Symposium on Saturn V/Apollo and Beyond, vol. I, American Astronautical Society, 1967, paper EN-8.

NASA SPACE VEHICLE MONOGRAPHS ISSUED TO DATE

SP-8001 (Structures)	Buffeting During Launch and Exit, May 1964
SP-8002 (Structures)	Flight-Loads Measurements During Launch and Exit, December 1964
SP-8003 (Structures)	Flutter, Buzz, and Divergence, July 1964
SP-8004 (Structures)	Panel Flutter, May 1965
SP-8005 (Environment)	Solar Electromagnetic Radiation, June 1965
SP-8006 (Structures)	Local Steady Aerodynamic Loads During Launch and Exit, May 1965
SP-8007 (Structures)	Buckling of Thin-Walled Circular Cylinders, (Revised, August 1968)
SP-8008 (Structures)	Prelaunch Ground Wind Loads, November 1965
SP-8009 (Structures)	Propellent Slosh Loads, August 1968
SP-8010 (Environment)	Models of Mars Atmosphere (1967), May 1968
SP-8011 (Environment)	Models of Venus Atmosphere (1968), December 1968
SP-8012 (Structures)	Natural Vibration Modal Analyses, September 1968
SP-8014 (Structures)	Entry Thermal Protection, August 1968
SP-8015 (Guidance and Control)	Guidance and Navigation for Entry Vehicles, November 1968
SP-8016 (Guidance and Control)	Effects of Structural Flexibility on Spacecraft Control Systems, April 1969.
SP-8018 (Guidance and Control)	Spacecraft Magnetic Torques, March 1969
SP-8019 (Structures)	Buckling of Thin-Walled Truncated Cones, September 1968.

NASA-Langley, 1969 —— 30